JACS
JOURNAL OF THE AMERICAN CHEMICAL SOCIETY
Article
pubs.acs.org/JACS

Photoelectrochemical and Impedance Spectroscopic Investigation of Water Oxidation with "Co−Pi"-Coated Hematite Electrodes

Benjamin Klahr,[†] Sixto Gimenez,[‡] Francisco Fabregat-Santiago,[‡] Juan Bisquert,[‡] and Thomas W. Hamann*,[†]

[†] Department of Chemistry, Michigan State University, East Lansing, Michigan 48824-1322, United States

[‡] Photovoltaics and Optoelectronic Devices Group, Departament de Física, Universitat Jaume I, 12071 Castelló, Spain

Supporting Information

ABSTRACT: Uniform thin films of hematite (α-Fe_2O_3) deposited by atomic layer deposition (ALD) coated with varying amounts of the cobalt phosphate catalyst, "Co−Pi," were investigated with steady-state and transient photoelectrochemical measurements and impedance spectroscopy. Systematic studies as a function of Co−Pi thickness were performed in order to clarify the mechanism by which Co−Pi enhances the water-splitting performance of hematite electrodes. It was found that under illumination, the Co−Pi catalyst can efficiently collect and store photogenerated holes from the hematite electrode. This charge separation reduces surface state recombination which results in increased water oxidation efficiency. It was also found that thicker Co−Pi films produced increased water oxidation efficiencies which is attributed to a combination of superior charge separation and increased surface area of the porous catalytic film. These combined results provide important new understanding of the enhancement and limitations of the Co−Pi catalyst coupled with semiconductor electrodes for water-splitting applications.

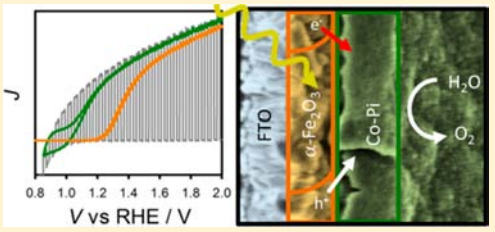

INTRODUCTION

An increasing global demand for energy, combined with an awareness of anthropogenic climate change, has fueled the search for abundant carbon neutral energy sources.[1] The sun illuminates the earth with an enormous amount of energy daily, where utilizing less than one percent of it has the potential of satisfying the world's energy demands.[2] Further, solar energy conversion represents a truly sustainable energy resource base that is expected to last billions of years. However, because solar energy is periodic for a given location while our energy demands are not, an efficient method must be developed to store the harvested solar energy. One attractive strategy to achieve this is through photoelectrochemical (PEC) water splitting, which stores energy in the bonds of H_2 and O_2. This concept was demonstrated in 1972 by Fujishima and Honda; however, no single material has yet been identified which contains all of the stability, cost, and efficiency requirements necessary for large-scale implementation.[3]

Hematite (α-Fe_2O_3) is one promising candidate for the water oxidation half reaction of PEC water splitting due to its adequate absorption of visible light up to 590 nm, very positive valence band energy, and good stability under water oxidation conditions.[4−8] Also, hematite is nontoxic and abundant which makes it a potential material for large-scale applications. However the combination of low minority charge carrier mobility and short lifetimes, resulting in a very short charge collection length, has historically prevented efficient solar energy conversion. The minority charge mobility mechanism is best described by small polaron hopping; thus, the short charge collection length is inherent to the chemical structure of hematite.[9,10] Recent advances in nanostructuring to deconvolute the light absorption and charge collection directions, combined with doping strategies, have partially overcome the short charge collection length limitations and have ignited renewed interest in this material.[4,11−15]

Another problem preventing efficient PEC water oxidation at hematite electrodes is the requirement of a large applied potential needed to produce a photocurrent. This large photocurrent onset potential is generally attributed to slow water oxidation kinetics at the hematite surface which competes with surface state recombination.[16−20] In order to reduce the required applied potential, various catalysts have been added to the hematite surface including IrO_2, cobalt ions, and the cobalt phosphate catalyst, "Co−Pi".[21−27] Co−Pi has specifically gained a lot of recent attention because it uses earth-abundant elements, shows effective water oxidation characteristics, and is stable over time due to its "self-healing" mechanism.[28−30] Consequently, it has also been applied to many potential photoanodes, including ZnO, $BiVO_4$, Si, and Fe_2O_3, and has shown improvements in both current onset potential and photocurrent density.[22−26,31−37] The reasons for this improvement, however, are not yet fully understood. Thus far, the increased performance has been attributed to accelerating the oxygen evolution kinetics,[22] increasing band bending,[26,38] facilitating charge separation,[22,23] and reducing surface state recombination.[25] Despite the cathodic shift frequently measured for Co−Pi-coated electrodes, Zhong and Gamelin

Received: July 2, 2012
Published: September 5, 2012

described evidence of a kinetic bottleneck on Co−Pi-coated hematite electrodes.[24] Thorough knowledge of the physical origin of both the improvement and limitation of water oxidation with Co−Pi-coated hematite electrodes is essential to guide further advances in catalyst and semiconductor design and integration into PEC water-splitting systems.

In this work, we employ photoelectrochemical measurements and impedance spectroscopy (IS) to investigate the effect of the Co−Pi catalyst on thin-film hematite electrodes. The thin-film hematite electrodes were prepared by atomic layer deposition (ALD)[39−41] and were subsequently coated with Co−Pi films by photoelectrodeposition.[24,25,36] These thin hematite films have been shown to be a good model system for studying the limitations of water oxidation at the hematite surface, thus allowing us to separate the effect of the catalyst from the bare electrode.[42,43] Also, the planar geometry of these films allowed us to perform a controlled thickness dependence study where increasing the amount of Co−Pi deposited uniformly increases the Co−Pi thickness in one dimension. The Co−Pi-coated hematite films were also analyzed by impedance spectroscopy and PEC experiments as a function of Co−Pi thickness to elucidate the factors controlling the enhanced performance of the Co−Pi-coated hematite electrode. These combined results provide new insight and allow for further development of a thorough mechanistic picture of this important system.

EXPERIMENTAL SECTION

Thin films of hematite were deposited on fluorine-doped tin oxide (FTO)-coated glass substrates (Hartford Glass, 12 Ω cm^{-2}) by ALD (Savannah 100, Cambridge Nanotech Inc.) using ferrocene as the metal precursor and wet ozone as the oxidation source. ALD is a process which employs alternating metal precursor and oxidation pulses each separated by a nitrogen purge such that chemistry only occurs in a self-limiting fashion where the previous precursor has adsorbed. The metal precursor was heated to 70 °C and pulsed for 20 s. After purging, the oxidation pulse was performed. The oxidation pulse consisted of a 0.015 s pulse of H_2O, immediately followed by a 1 s pulse of ozone (~4.5% by weight O_3 in ultrahigh purity O_2 produced by Yanco Industries ozone generator), followed by a 5 s purge time. This cycle was performed 10 times to create 1 oxidation macrocycle. Integrating water with O_3 has been found to be necessary for uniform deposition of hematite in our system. Films were prepared by 1000 ALD cycles and measured to be ~60 nm by absorption measurements (Perkin-Elmer, Lambda 35 with a Labsphere integrating sphere) corrected for reflection as described previously, as well as ellipsometric measurements (Horiba Jobin Yvon, Smart-SE).[41] Films were characterized by Raman spectroscopy and X-ray diffraction (XRD) of these films previously.[41] Hematite electrodes were masked with a 60 μm Surlyn film (Solaronix) with a 0.28 cm^2 hole to define the active area and to prevent scratching of the thin films. Surlyn films were adhered to the electrodes by heating to 120 °C. The protected hematite films were clamped to a custom-made glass electrochemical cell. A homemade saturated Ag/AgCl electrode was used as a reference and was frequently calibrated to a commercial saturated calomel reference electrode (Koslow Scientific). Potentials vs Ag/AgCl were converted to the reversible hydrogen electrode (RHE) scale by the equation $E_{RHE} = E_{Ag/AgCl} + 0.197V + (0.059V)$pH. A high surface area platinum mesh was used as the counterelectrode.

Co−Pi catalyst films were deposited onto hematite by photoassisted electrodeposition.[25] Hematite electrodes were immersed in a solution containing 0.5 mM $Co(NO_3)_2{\cdot}6H_2O$ in a 0.1 M phosphate buffer (pH 6.9). A bias of 0.9 V vs RHE was applied under illumination. The thickness of the Co−Pi layer was controlled by varying the amount of charge allowed to pass during the deposition. For the electrodes reported herein, 5 thicknesses were prepared by allowing 1, 2, 15, 45, and 90 mC cm^{-2} to pass. After the catalyst was deposited, the electrodes were lightly rinsed with DI water to remove any excess cobalt ions. Co−Pi-coated hematite electrodes were prepared separately for SEM examination. After Co−Pi was photoelectrodeposited, electrodes were allowed to air-dry. SEM images were taken on an Auriga CrossBeam FIB-SEM (Carl Zeiss Microscopy).

The water oxidation properties of the catalyst-coated hematite films were then examined in contact with an aqueous solution buffered at pH 6.9 using a 0.1 M phosphate buffer containing 200 mM KCl as a supporting electrolyte. The pH was determined with a Fisher Scientific Accumet pH meter. Impedance spectroscopic and photoelectrochemical measurements were made with an Eco Chemie Autolab potentiostat coupled with Nova electrochemical software. Impedance data were gathered using a 10 mV amplitude perturbation of between 10,000 and 0.01 Hz. Data were fit using Zview software (Scribner Associates). The light source was a 450 W Xe arc lamp. An AM 1.5 solar filter (Sciencetech Inc.) was used to simulate sunlight at 100 mW cm^{-2}. All photoelectrochemical measurements were performed by shining light from the substrate−electrode (SE) interface which avoids competitive light absorption of the Co−Pi. Light-chopping $J-V$ curves were measured at a rate of 75 mV/s. The light was chopped using a computer-controlled ThorLabs solenoid shutter which was set to activate every 266 ms such that the light was turned on or off every 20 mV. Steady-state $J-V$ curves were measured at a scan rate of 5 mV/s.

Oxygen was detected by using an Ocean Optics spectrometer which probed the fluorescent decay of the FOSPOR patch. The FOSPOR patch was placed in solution which filled an airtight cell. The cell was filled so that very little headspace existed. The solution was stirred vigorously so that the O_2 measurement would be as close to real time as possible. Measurements were made under 4 sun illumination at 1.25 V vs RHE to increase oxygen production and reduce noise. In the calculation of the faradaic efficiency, the assumption was made that no oxygen diffused into the very small headspace during the time scale of these experiments.

While these experiments were performed multiple times with many electrodes, only three different, but nominally identical electrodes were used to collect the photoelectrochemical data shown here: one for current transient and $J-V$ curves, one for EIS measurements, and one for O_2 measurements. The use of one electrode for each experiment allowed us to control for any small differences between bare electrodes. For experiments with varying amounts of Co−Pi, the Co−Pi was removed by applying a potential of 0.55 V vs RHE under dark conditions which slowly removed the Co−Pi film. After the Co−Pi was removed, the electrodes were examined to ensure that the performance was consistent with a bare electrode before applying Co−Pi for the next experiment.

RESULTS AND DISCUSSION

Thin-film hematite electrodes were coated with varying thicknesses of the Co−Pi catalyst via photoelectrodeposition.[24,25,36] At the potential applied during the deposition (0.9 V vs RHE) steady-state water oxidation does not occur with or without the Co−Pi catalyst (*vide infra*); thus, any charge passed is assumed to be due to deposition of the catalyst. Film thicknesses can then be estimated by assuming that a single passed electron deposits one cobalt atom with surrounding ligands which occupies a volume of approximately 125 $Å^3$.[28] The thicknesses of the Co−Pi layers deposited by 1, 2, 15, 45, and 90 mC cm^{-2} were calculated to be 8, 15, 113, 337, and 675 nm, respectively. Co−Pi-coated hematite films were analyzed by SEM to measure thickness and morphology; all of the films were found to be flat and uniform. Figure 1 shows a hematite film coated with Co−Pi by allowing 90 mC cm^{-2} to pass. This film was allowed to air dry immediately after the deposition. Assuming a 90° plane of the edge of the Co−Pi, with respect to the underlying hematite, and a viewing angle of 45°, the thickness of this film is estimated to be ~425 nm. This thickness is largely the same throughout the film and on other films prepared by depositing 90 mC cm^{-2} Co−Pi, which is

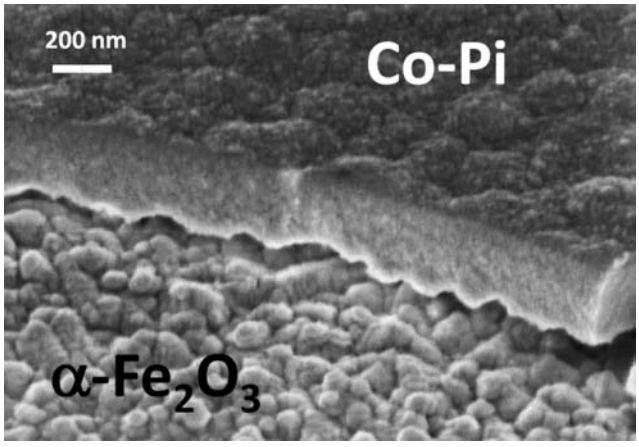

Figure 1. SEM image of a Co−Pi film deposited by passing 90 mC cm^{-2}. Sample was air-dried immediately after deposition. The viewing angle is 45°.

considerably less than the calculated thickness of 675 nm. Therefore, either the size of the cobalt cluster represents an overestimation, or not all of the charge passed is productive at depositing the film. In order to avoid ambiguity in the discussion of the Co−Pi films, the thicknesses will be referred to by the amount of charge passed (mC cm^{-2}) in the deposition, which was found to be roughly proportional to the film thickness. The morphology of the Co−Pi shown in the SEM image is consistent throughout the film.

Current density, *J*, vs applied voltage, *V*, curves measured under 1 sun (100 mW cm^{-2}) illumination for a bare hematite electrode and the same hematite electrode coated with the varying thicknesses of the Co−Pi catalyst can be seen in Figure 2a. Steady-state current measurements were also performed where the photocurrent was sampled after stabilizing over several minutes for individual potentials (see Supporting Information [SI]). It was found that the steady-state current densities are equal to the current densities of the cathodic scan of the *J*−*V* curves, thus confirming that the *J*−*V* measurements presented herein represent steady-state behavior. The faradaic efficiency of the *J*−*V* curves was also measured by a fluorescent O_2 sensor. The O_2 concentration was measured at 1.25 V vs RHE which showed an increase in detected O_2 with increasing Co−Pi thickness for Co−Pi amounts up to 15 mC cm^{-2}; the O_2 detected was consistent with ∼100% faradaic efficiency when considering the number of coulombs that have passed (SI). Clearly, the addition of Co−Pi to the hematite improves the water oxidation efficiency. Figure 2b shows a semi-logarithmic plot of the cathodic shift of the of the *J*−*V* curves in Figure 2a by sampling the potential needed to sustain a 200 μA cm^{-2} current density. The shift in photocurrent onset potential increases with Co−Pi thickness, quickly reaching a saturated shift of ∼0.23 V for Co−Pi thicknesses greater than 15 mC cm^{-2}. This behavior is consistent with experiments examining Co−Pi on planar FTO-coated glass, which was attributed to an increase in the number of active catalytic sites.[28] This trend, however, was not observed in a recent study examining Co−Pi deposited on high surface area hematite.[25] Thus, the simple explanation of increasing the number of active catalytic sites does not adequately describe the enhanced performance of the Co−Pi−hematite system. An alternative explanation is discussed below. In addition to the shift of the *J*−*V* curve, a slight increase in the photocurrent density at

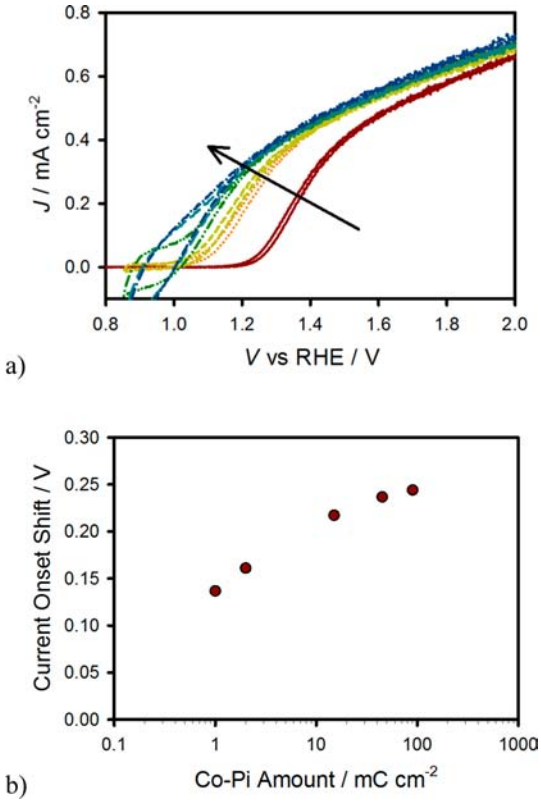

Figure 2. (a) *J*−*V* curves measured at 5 mV/s under 1 sun illumination of a bare α-Fe_2O_3 electrode (red solid line) and the same electrode with 1 (orange dotted line), 2 (yellow short dashed line), 15 (green dashed double dotted line), 45 (teal long dashed line), and 90 (blue dashed single dotted line) mC cm^{-2} Co−Pi catalyst in contact with a pH 6.9 buffered aqueous solution under 1 sun illumination. (b) Potential shift of the current onset relative to the bare electrode measured at 200 mA cm^{-2}.

potentials positive of 1.4 V vs RHE is observed. This enhancement, however, is independent of Co−Pi thickness. The improved PEC performance is generally consistent with previous reports of Co−Pi-coated hematite electrodes.[22,25,26]

While steady-state measurements were performed, it became apparent that increasing the Co−Pi thickness required an increasing amount of time to reach steady state. Current transients were therefore measured in response to turning on (anodic) and off (cathodic) 1 sun illumination at a constant potential. Examples of anodic and cathodic current transients for different thicknesses of Co−Pi on hematite electrodes can be seen in a and b of Figure 3, respectively, at an applied bias of 1.05 V vs RHE. As shown previously for bare hematite electrodes,[42] at potentials negative of the current onset potential (such as 1.05 V vs RHE), an anodic spike in current is visible when the light is turned on which quickly decays to the steady-state current density. When the light is turned off, a cathodic spike in current is observed which quickly decays to J_0. These spikes have been attributed to the charging (trapping of holes) and discharging of surface states, or oxidizing and reducing surface species.[42] Analogous behavior is observed when Co−Pi is added to the surface of hematite; however, the amount of charge passed in the transients obviously increases with Co−Pi thickness. This suggests that the processes governing the transients are controlled by the Co−Pi. The anodic transients are attributed to the oxidation of Co(III) in the Co−Pi catalyst layer to Co(IV) by photogenerated holes in

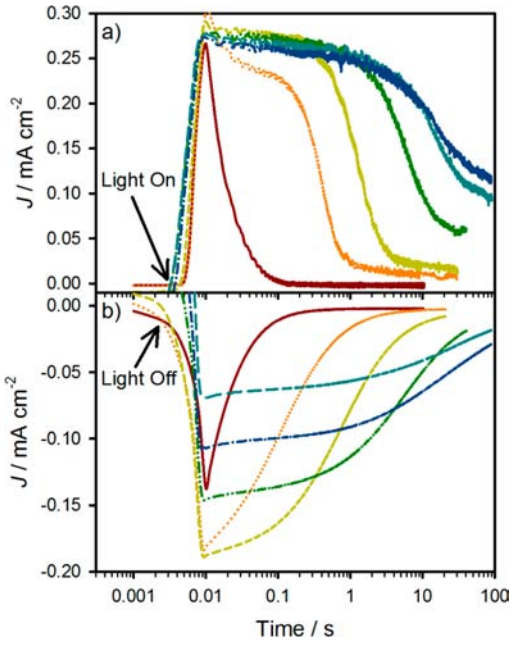

Figure 3. (a) Anodic and (b) cathodic transients measured for a bare hematite electrode (red solid line) and the same electrode with 1 (orange dotted line), 2 (yellow short dashed line), 15 (green dashed double dotted line), 45 (teal long dashed line) and 90 (blue dashed single dotted line) mC cm^{-2} Co−Pi catalyst in contact with a pH 6.9 buffered aqueous solution under 1 sun illumination at an applied bias of 1.05 V vs RHE.

the valence band. This assignment is based on the recent observation of Co(IV) by EPR from Co−Pi which was electrodeposited during water oxidation.[44] Since such a large amount of charge is passed, and the quantity scales with thickness of the Co−Pi layer, the catalyst film must have the Co(IV) species distributed throughout. This indicates efficient diffusion of holes through the catalyst film via charge transfer from/to the cobalt centers, consistent with recent self-exchange measurements of Co−Pi using a model cubane molecule.[45] The cathodic transient measured after turning the light off is attributed to the reduction of Co(IV) to Co(III) by electrons from the conduction band of the hematite (i.e., recombination). The recombination time scale indicated by the cathodic transients generally scales with Co−Pi thickness, with thicker films requiring a longer time to reduce all the stored Co(IV), however, in a less straightforward manner than the anodic transients. The initial current peak is the same for the 1 and 2 mC cm^{-2} Co−Pi films, then decreases monotonically with increasing Co−Pi thickness. The peak current should be proportional to the concentration of electrons in the conduction band and electron acceptors, [Co(IV)], at the interface, and the total charge passed, proportional to the total number of Co(IV) centers stored. At a given applied bias it is not expected that changing the Co−Pi thickness would change the concentration of electrons in the conduction band immediately after turning off the light, assuming a constant conduction band position (see below). Therefore, the decreasing cathodic peak heights can be attributed to decreasing concentrations of Co(IV) for Co−Pi thicknesses larger than 2 mC cm^{-2} at an applied bias of 1.05 V vs RHE. This corresponds to the same Co−Pi thickness where water oxidation occurs at 1.05 V vs RHE. Since water oxidation represents a parallel pathway that would deplete the Co−Pi film of Co(IV), it makes sense that increasing water oxidation kinetics would lead to a decreased concentration of Co(IV) in the film. In order to test this hypothesis, we also measured cathodic current transients at 0.95 V vs RHE where water oxidation does not occur for 1, 2, or 15 mC cm^{-2} films (see Figure S4 in SI). At this potential, the initial peak current was the same for all films, and the total charge passed is clearly proportional to film thickness, as expected. In addition, cathodic current transients were measured as a function of applied potential (see Figure S5 in SI). The initial peak current drops rapidly with increasing applied bias as expected since increasing the applied bias should decrease the conduction band concentration at the electrode surface as well as decrease Co(IV) due to increasing water oxidation.

Light-chopping experiments were also performed for electrodes with varying thicknesses of Co−Pi. Figure 4 shows a *J*−*V*

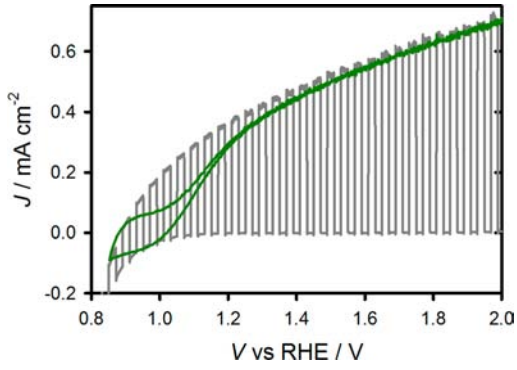

Figure 4. *J*−*V* curve for a hematite electrode coated with 15 mC cm^{-2} Co−Pi measured under constant 1 sun illumiation (green line) and under chopped 1 sun illumination.

curve measured under chopped and constant 1 sun illumination for a 15 mC cm^{-2} Co−Pi-coated hematite electrode. The maximum current of the chopped light *J*−*V* is approximately linear which is reached instantaneously upon turning the light on. This behavior is similar to previous reports of hematite electrodes measured in contact with an electrolyte containing a fast redox shuttle.[42,46,47] Two different regions are observed when comparing the chopped-light *J*−*V* curve to the steady-state *J*−*V* curve. One is at potentials positive of ∼1.4 V vs RHE where the instantaneous photocurrent measured by chopped light is equal to the steady-state *J*−*V* curve. The other region is between 0.85 and 1.4 V vs RHE where the instantaneous photocurrent measured by light chopping is much higher than the steady-state photocurrent. In other words, at these potentials, charge is being transferred to and stored in the Co−Pi film without steady-state water oxidation occurring. This "trapping" in the Co−Pi film presents an opportunity for recombination of electrons in the conduction band and Co(IV) to produce Co(III). This balance of charge separation and recombination may account for the different behavior observed for high aspect ratio electrodes.[25] Chopped-light *J*−*V* curves measured for different Co−Pi thicknesses can be seen in SI.

IS measurements were also performed for electrodes with varying thicknesses of Co−Pi. An example of a Nyquist plot measured under illumination for a bare hematite electrode and a hematite electrode coated with 15 mC cm^{-2} of Co−Pi at 1.25 V vs RHE can be seen in Figure 5. Around the photocurrent onset, two semicircles are clearly visible for both bare and Co−Pi-coated hematite electrodes. The low-frequency (high

dx.doi.org/10.1021/ja306427f | J. Am. Chem. Soc. 2012, 134, 16693−16700

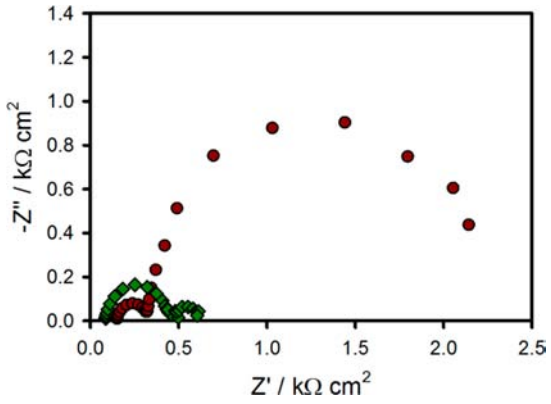

Figure 5. Nyquist plots measured under illumination of a bare hematite electrode (red circles) and with 15 mC cm^{-2} Co−Pi catalyst (green triangles) measured at 1.25 V vs RHE.

impedance) semicircle is clearly much smaller for Co−Pi-coated electrodes compared to the bare electrodes. At more positive potentials (>1.25 V vs RHE), the low-frequency semicircle disappears for Co−Pi-coated hematite electrodes.

The general equivalent circuit, EC, used to interpret the IS data is shown in Figure 6a. The proposed circuit includes the

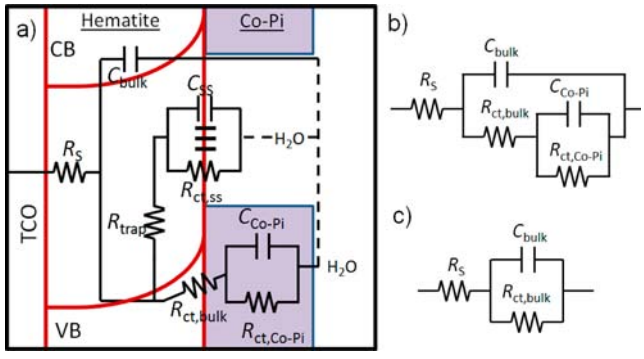

Figure 6. (a) Proposed full equivalent circuit used for interpretation of hematite electrodes coated with Co−Pi catalyst. (b) Simplified equivalent circuit used for interpretation of Co−Pi-coated Fe_2O_3. (c) Randles' circuit used when only one semicircle is visible.

circuit established previously for a bare hematite electrode under illumination which has also recently been modeled in detail.[43,48] This EC consists of the capacitance of the bulk hematite, C_{bulk}, charge transfer resistance from the valence band of the hematite, $R_{ct,bulk}$, a resistance which is related to the rate of trapping holes in surface states, R_{trap}, a capacitance of the surface states, C_{ss}, and charge transfer from the surface states, $R_{ct,ss}$.[43] Additional electrical components were added to account for the Co−Pi layer including the capacitance of the Co−Pi layer, C_{Co-Pi}, and charge transfer resistance from the Co−Pi layer, $R_{ct,Co-Pi}$. Clearly, the full EC shown in Figure 6a cannot be used to unambiguously fit the IS data for coated Co−Pi. One thing that allowed us to simplify the equivalent circuit was independent examination of the low-frequency semicircle; the capacitance of this feature increases approximately linearly with increasing Co−Pi thickness (shown and discussed below). This allowed assignment of this capacitance to C_{Co-Pi}, thus simplifying the EC to that shown in Figure 6b.

The impedance spectra of hematite electrodes with varying amounts of Co−Pi deposited, measured under 1 sun illumination, were fit to the EC shown in Figure 6b. Figure 7a shows plots of C_{Co-Pi} vs applied potential for the different

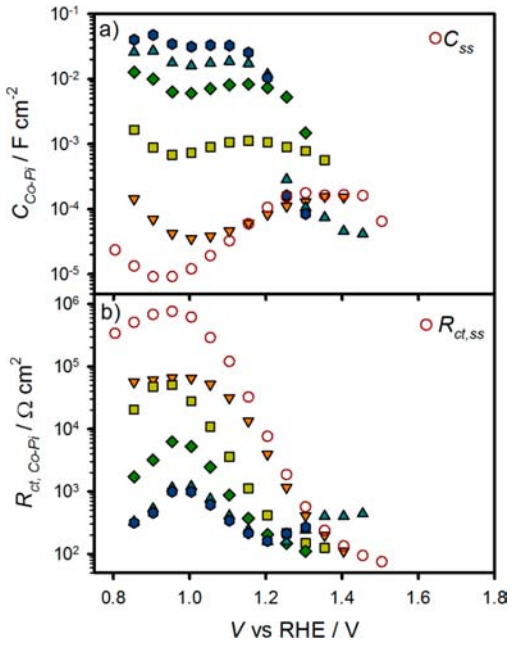

Figure 7. (a) C_{Co-Pi} and (b) $R_{ct,Co-Pi}$ values fit from impedance response of hematite electrodes with 1 (orange triangles pointing down), 2 (yellow squares), 15 (green diamonds), 45 (teal triangles pointing up), and 90 mC cm^{-2} (blue hexagons) Co−Pi deposited. Bare hematite fitting parameters of (a) C_{ss}, (b) $R_{ct,ss}$ are shown for comparison (red open circles).

thicknesses of Co−Pi deposited on the hematite film. The C_{Co-Pi} increases with thickness which is consistent with the assignment of this capacitance to the chemical capacitance of Co−Pi. This is also consistent with the trend of increasing charge passed before reaching a steady-state current in the current transient measurements displayed in Figure 3. Evidence of a capacitance due to the Co−Pi is also observed by performing $J-V$ measurements at various scan rates of Co−Pi-coated hematite electrodes in a recent study by Zhong et al.[24] The measurement of C_{Co-Pi} provides direct and clear evidence of hole storage throughout the Co−Pi catalyst film. The values for $R_{ct,Co-Pi}$, shown in Figure 7b, are also related to the Co−Pi layer thickness; the resistance decreases with increasing Co−Pi thickness. When deposited on FTO, Co−Pi is known to be a porous material which shows a decrease in the required applied potential with an increasing amount of the catalyst.[28] The dependence of the decreasing $R_{ct,Co-Pi}$ with Co−Pi thickness is also consistent with the Co−Pi being a porous material. For all Co−Pi thicknesses, $R_{ct,Co-Pi}$ decreases exponentially with increasing potential. Similar to the current transients discussed above, there are two clear regions that are observed in the Nyquist plots. One is at potentials less than 1.4 V vs RHE which shows two clear semicircles where the contribution of the Co−Pi can be observed. However, at potentials greater than 1.4 V vs RHE the low-frequency capacitive feature disappears, and meaningful values for C_{Co-Pi} and $R_{ct,Co-Pi}$ cannot be calculated. For these data, a simple Randles' circuit (Figure 6c) is used to fit the impedance spectra and calculate values for $R_{ct,bulk}$ and C_{bulk}. The low-frequency semicircle also disappears for bare hematite electrodes at more positive potentials (>1.5 V vs RHE), which has recently been attributed to a hole transfer

dx.doi.org/10.1021/ja306427f | J. Am. Chem. Soc. 2012, 134, 16693−16700

from the surface states of iron oxide to solution which is not the rate-limiting step of water oxidation.[43] Similarly, we propose that at potentials where this low-frequency capacitive feature measured on Co−Pi-coated electrodes disappears, charge transfer from the Co−Pi to solution is not the rate-limiting step. This is the cause of the independence of photocurrent measured at potentials positive of ∼1.4 V vs RHE for increasing Co−Pi thickness. At these positive potentials, the photocurrent is controlled by the number of holes that reach the hematite surface for both bare and Co−Pi-coated hematite electrodes.[47]

Values of $R_{ct,bulk}$, which represent the charge transfer from the hematite to the Co−Pi catalyst, can be found in Figure 8. $R_{ct,bulk}$

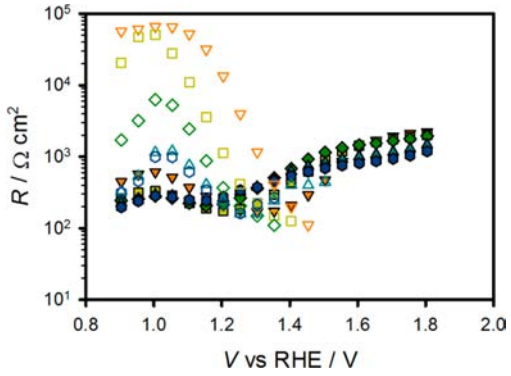

Figure 8. $R_{ct,bulk}$ (solid shapes) and $R_{ct,Co-Pi}$ (open shapes) measured for a hematite electrode coated with 1 (orange pointing down triangles), 2 (yellow squares), 15 (green diamonds), 45 (teal pointing up triangles), and 90 mC cm^{-2} (blue hexagons) Co−Pi.

is on the order of 10^2−10^3 Ω cm^2. These resistances are comparable to when a fast redox shuttle such as $[Fe(CN)_6]^{3-/4-}$ is used as a hole scavenger as reported previously.[42] This is consistent with having fast charge transfer of holes from the valence band of hematite to the Co−Pi. At potentials negative of the current onset potential, $R_{ct,Co-Pi}$ is much higher than $R_{ct,bulk}$. This is consistent with light-chopping experiments where, at these low applied potentials, charge transfer to Co−Pi is facile; yet water oxidation from the Co−Pi does not occur according the steady-state J−V curves and O_2 measurements. $R_{ct,Co-Pi}$ is also included in the same graph to emphasize which resistance is the limiting resistance at a given potential. The total resistance, R_{tot}, was calculated (R_s + $R_{ct,Co-Pi}$ + $R_{ct,bulk}$) and compared to the resistance derived from the J−V curve ($R_{tot} = A_s(dV/dJ)$). A plot of R_{tot} derived from both impedance and J−V results can be seen in SI. The overlap of the R_{tot} determined from IS and the J−V curve shows how $R_{ct,bulk}$ and $R_{ct,Co-Pi}$ determine the shape of the J−V curve.

Plots of C_{bulk} values can be seen in Figure 9a. These values are essentially constant for all thicknesses of Co−Pi and the bare hematite electrode. Mott−Schottky (MS) plots were prepared from these C_{bulk} values and are displayed in Figure 9b. As shown previously for bare hematite electrodes, MS plots show a horizontal shift which we attribute to band unpinning by surface-trapped holes.[42,43] This band unpinning is not observed in dark conditions (see SI). The MS plots measured with the Co−Pi-coated hematite electrode shows a much more linear behavior compared to the bare electrode, suggesting that band unpinning is reduced. This is consistent with photogenerated holes being transferred to the Co−Pi layer instead of being trapped in surface states, as shown directly by the C_{Co-Pi}. Also, the flat band potential extrapolated from both bare and

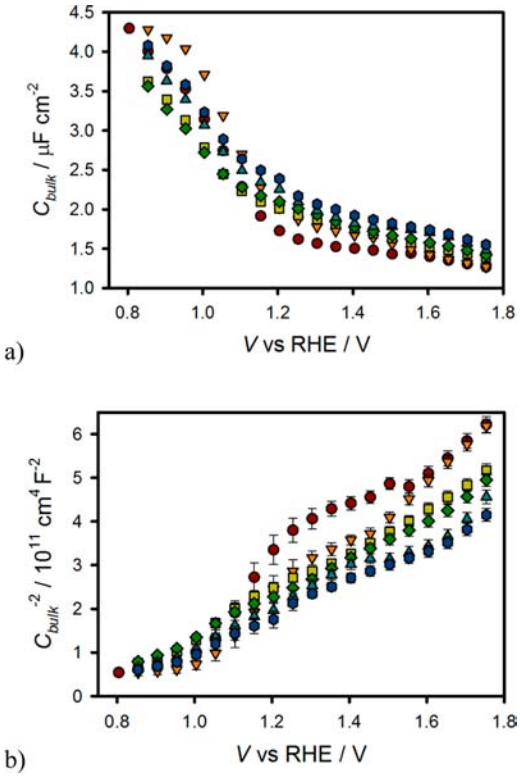

Figure 9. (a) C_{bulk} values fit from IS data of a bare hematite electrode (red circles) and the same electrode with 1 (orange pointing down triangles), 2 (yellow squares), 15 (green diamonds), 45 (teal pointing up triangles), and 90 (blue hexagons) mC cm^{-2} Co−Pi deposited. (b) Mott−Schottky plot prepared from C_{bulk} values determined by IS. Also included are values measured for a bare electrode in the dark (black circles).

Co−Pi-coated hematite electrodes is the same, within the error of this measurement, suggesting that Co−Pi does not shift the band positions. This is in contrast with a recent report that has suggested the primary role of Co−Pi on Co−Pi-coated hematite electrodes is increased band bending.[26] The flat band potential and dopant density extracted from the MS plots are in good agreement with previous reports of thin-film hematite electrodes.[41−43]

To summarize the results presented above, deposition of the Co−Pi catalyst to planar hematite electrodes produces a favorable shift in the photocurrent onset potential. This shift increases with increasing Co−Pi thickness up to a saturated value of ∼240 mV. Transient photocurrent and chopped-light measurements showed that valence band holes in hematite efficiently oxidize Co(III) in the Co−Pi film to Co(IV). The transient anodic and cathodic photocurrent measurements, as well as the C_{Co-Pi} measured by IS, as a function of Co−Pi thickness clearly show that photogenerated holes from hematite can be stored as Co(IV) throughout the Co−Pi layer. Also, the decreasing $R_{ct,Co-Pi}$ with increasing Co−Pi thickness showed that the Co−Pi is porous and has catalytically active sites throughout. The resistances extracted from the IS measurements accurately account for the steady-state J−V behavior of Co−Pi-coated hematite electrodes which we further showed correspond to unity faradaic efficiency of oxygen generation. Therefore, these results clearly demonstrate that water oxidation occurs predominately from the Co−Pi film, not the hematite surface. Cathodic current transients show that

dx.doi.org/10.1021/ja306427f | J. Am. Chem. Soc. 2012, 134, 16693−16700

recombination of electrons from the hematite conduction band to Co(IV) is also a fast process, which decreases with increasing Co−Pi thickness. The improved photocurrent onset potential with increasing thickness of Co−Pi can therefore be accounted for by improved charge separation since an increasing fraction of Co(IV) is distributed throughout the Co−Pi film away from the hematite surface. It was also found that at potentials >∼1.4 V vs RHE, the photocurrent does not increase with increasing Co−Pi thickness. We propose that, at these potentials, there are enough adjacent Co(IV) active sites that, when a hole reaches the hematite/Co−Pi interface, it can be immediately turned into faradaic photocurrent (oxygen). This is consistent with current transients which instantaneously reach the maximum current upon illumination, as well as IS which shows the disappearance of the low-frequency semicircle attributed to trapping of holes, be it in surface states for a bare electrode or in the Co−Pi for a Co−Pi-coated electrode.[42,43]

We now are in a position to compare our findings with the literature. The cathodic shifts in photocurrent onset potential measured in this study are higher than the ∼180 mV shifts observed when Co−Pi is deposited on hematite electrodes with higher surface area.[24−26] Also, for high surface area hematite, the shift did not increase with Co−Pi thickness and required the optimization of thin Co−Pi layers.[24,25] On the basis of our results, a higher surface area hematite electrode would provide a larger source of electrons to recombine with the Co(IV) since thicker layers of Co−Pi may bridge two regions of hematite and thus not produce better charge separation. In addition, it is worth pointing out that measurements on structured hematite films are performed by shining light from the front (electrode) side, whereas we shine light from the back (FTO substrate) side. Since Co−Pi films broadly absorb visible light,[26] the measurements of thick Co−Pi films on structured electrodes are difficult to interpret since the decreasing light absorption by the hematite with thicker Co−Pi films is convoluted with the effect of the Co−Pi film. Although the thin films used herein are not practical for achieving the highest photocurrents, the use of such films allowed us to perform a controlled thickness dependence which showed an increasing performance with increasing Co−Pi thickness, a trend consistent with Co−Pi on FTO.[28] Transient absorption measurements have also recently been employed to determine the role of Co−Pi in enhancing the performance of a variety of hematite electrodes.[26,38] These authors suggested that Co−Pi acts as an electron acceptor which causes increased band bending and enhancement of charge separation within the hematite, and not hole transfer to the Co−Pi. This interpretation implies that water oxidation occurs at the hematite surface and not through the Co−Pi. Our measurements of C_{bulk} however, including their representation in Mott−Schottky plots, indicate that the band bending is essentially constant upon the addition of Co−Pi. Further, as described above, our measurements clearly show efficient hole transfer from hematite to Co−Pi and that water oxidation is occurring predominately from the Co−Pi catalyst, not the hematite surface. Thus, the results presented herein are in stark contrast to several recent reports. We note that the hematite films being compared were prepared in different fashion and geometry, and very different techniques were employed to interrogate them, which may account for these differences in interpretation.

CONCLUSIONS

Uniform thin films of hematite were coated with varying amounts of the Co−Pi and investigated with a variety of steady-state and transient photoelectrochemical measurements and impedance spectroscopy. These systematic studies allowed for the identification of the mechanism by which Co−Pi enhances the water-splitting performance of hematite electrodes. The Co−Pi catalyst efficiently collects and stores photogenerated holes from the hematite electrode. This charge separation reduces recombination which results in lower photocurrent onset potentials and hence water oxidation efficiency. One way of rationalizing the better water oxidation efficiency with increasing charge separation is through a bimolecular water oxidation mechanism which requires the oxidation of two adjacent cobalt atoms before oxidizing water such as has been proposed for Co−Pi on FTO electrodes.[28] In this case, long-lived Co(IV) species are necessary in order to move to an adjacent Co(IV). This framework allows several analogies to be drawn between the bare hematite electrode and the Co−Pi-coated electrode. Both require the oxidation of a water oxidation active site to an intermediate species before facile water oxidation occurs.[42] The accumulation of intermediates at illuminated bare hematite surface in contact with water has been measured in several recent papers by photoelectrochemical impedance spectroscopy,[17,42,43] intensity modulated photocurrent spectroscopy,[27] transient absorption spectroscopy,[20,38,50] and near edge X-ray absorption fine structure measurements.[51] In the case of a bare electrode this is possibly the oxidation of an Fe(III)-hydroxide to an Fe(IV)-oxo intermediate, although the identity of this Fe(IV)-oxo intermediate has not yet been confirmed.[42,52,53] In the case of Co−Pi, this is likely the oxidation of a Co(III)-hydroxyl to a Co(IV)-oxo intermediate (Figure 10).[28,44] The water oxidation

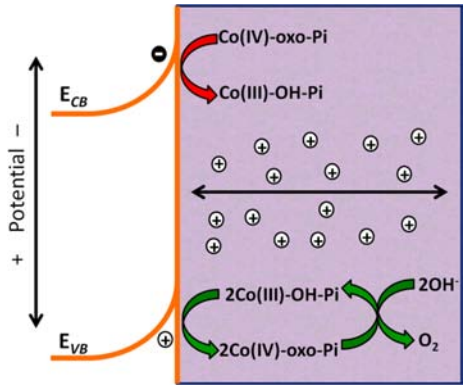

Figure 10. Diagram of a Co−Pi-coated hematite electrode under illumination and applied bias; the mechanism of Co−Pi is adopted from reference 49. The chemical capacitance of the Co−Pi film is attributed to the distribution of holes throughout the film.

intermediates of both bare and Co−Pi-coated hematite electrodes are both, however, subject to recombination or reduction by electrons in the conduction band. For both bare and Co−Pi-coated electrodes, this recombination is turned off with an applied potential and high band bending. Co−Pi-coated hematite electrodes differ from bare hematite electrodes by efficiently separating charge and thereby reducing recombination and allowing longer lived holes as Co(IV) species. Despite this improved charge separation, Co−Pi is not immune to recombination from electrons in the conduction band. For

dx.doi.org/10.1021/ja306427f | J. Am. Chem. Soc. 2012, 134, 16693−16700

Co−Pi to improve photoanodes further, recombination of electrons from the conduction band must be reduced.

■ ASSOCIATED CONTENT

Supporting Information

Plots of steady-state photocurrent measurements, oxygen evolution measurements, cathodic current transients, chopped-light $J-V$ curves, total resistances derived from IS and $J-V$ curves and Mott−Schottky plots. Results of PEC and IS response to variations in light intensity. This material is available free of charge via the Internet at http://pubs.acs.org.

■ AUTHOR INFORMATION

Corresponding Author

hamann@chemistry.msu.edu

Notes

The authors declare no competing financial interest.

■ ACKNOWLEDGMENTS

T.W.H. thanks the National Science Foundation (CHE-1150378) for support of this research. J.B. and F.F.S. acknowledge support by projects from Ministerio de Industria y Competitividad (MINECO) of Spain (Consolider HOPE CSD2007-00007) and Generalitat Valenciana (PROMETEO/2009/058, and the "Institute of Nanotechnologies for Clean Energies", under Project ISIC/2012/008). F.F.S. thanks the funding of University Jaume I- Bancaixa (Grant P1·1B2011-50). S.G. acknowledges support by MINECO of Spain under the Ramon y Cajal programme.

■ REFERENCES

(1) Moomow, W.; Yamba, F.; Kamimoto, M.; Maurice, L.; Nyboer, J.; Urama, K.; Weir, T. In *IPCC Special Report on Renewable Energy Sources and Climate change Mitigation*; Edenhofer, O., Pichs-Madruga, R., Sokona, Y., Seyboth, K., Matschoss, P., Kadner, S., Zwickel, T., Eickemeier, P., Hansen, G., Schlömer, S., von Stechow, C., Eds.; Cambridge University Press: United Kingdom and New York, NY, USA, 2011.

(2) Lewis, N. S.; Nocera, D. G. *Proc. Natl. Acad. Sci. U.S.A.* **2006**, *103*, 15729.

(3) Fujishima, A.; Honda, K. *Nature* **1972**, *238*, 37.

(4) Lin, Y. J.; Zhou, S.; Sheehan, S. W.; Wang, D. W. *J. Am. Chem. Soc.* **2011**, *133*, 2398.

(5) Kennedy, J. H.; Frese, K. W. *J. Electrochem. Soc.* **1978**, *125*, 709.

(6) Marusak, L. A.; Messier, R.; White, W. B. *J. Phys. Chem. Solids* **1980**, *41*, 981.

(7) Hardee, K. L.; Bard, A. J. *J. Electrochem. Soc.* **1977**, *124*, 215.

(8) Hamann, T. W. *Dalton Trans.* **2012**, *41*, 7830.

(9) Goodenough, J. B. *Prog. Solid State Chem.* **1971**, *5*, 145.

(10) Kerisit, S.; Rosso, K. M. *J. Chem. Phys.* **2007**, *127*, 124706.

(11) Kay, A.; Cesar, I.; Gratzel, M. *J. Am. Chem. Soc.* **2006**, *128*, 15714.

(12) Lin, Y.; Xu, Y.; Mayer, M. T.; Simpson, Z. I.; McMahon, G.; Zhou, S.; Wang, D. *J. Am. Chem. Soc.* **2012**, *134*, 5508.

(13) Bjorksten, U.; Moser, J.; Gratzel, M. *Chem. Mater.* **1994**, *6*, 858.

(14) Duret, A.; Gratzel, M. *J. Phys. Chem. B* **2005**, *109*, 17184.

(15) He, J.; Parkinson, B. A. *ACS Combi. Sci.* **2011**, *13*, 399.

(16) Dareedwards, M. P.; Goodenough, J. B.; Hamnett, A.; Trevellick, P. R. *J. Chem. Soc., Faraday Trans. 1* **1983**, *79*, 2027.

(17) Upul Wijayantha, K. G.; Saremi-Yarahmadi, S.; Peter, L. M. *Phys. Chem. Chem. Phys.* **2011**, *13*, 5264.

(18) Peter, L. M.; Wijayantha, K. G. U.; Tahir, A. A. *Faraday Discuss.* **2012**, *155*, 309.

(19) Cowan, A. J.; Barnett, C. J.; Pendlebury, S. R.; Barroso, M.; Sivula, K.; Grätzel, M.; Durrant, J. R.; Klug, D. R. *J. Am. Chem. Soc.* **2011**, *133*, 10134.

(20) Pendlebury, S. R.; Barroso, M.; Cowan, A. J.; Sivula, K.; Tang, J. W.; Gratzel, M.; Klug, D.; Durrant, J. R. *Chem. Commun.* **2011**, *47*, 716.

(21) Tilley, S. D.; Cornuz, M.; Sivula, K.; Grätzel, M. *Angew. Chem., Int. Ed.* **2010**, *49*, 6405.

(22) McDonald, K. J.; Choi, K. S. *Chem. Mater.* **2011**, *23*, 1686.

(23) Zhong, D. K.; Sun, J. W.; Inumaru, H.; Gamelin, D. R. *J. Am. Chem. Soc.* **2009**, *131*, 6086.

(24) Zhong, D. K.; Gamelin, D. R. *J. Am. Chem. Soc.* **2010**, *132*, 4202.

(25) Zhong, D. K.; Cornuz, M.; Sivula, K.; Graetzel, M.; Gamelin, D. R. *Energy Environ. Sci.* **2011**, *4*, 1759.

(26) Barroso, M.; Cowan, A. J.; Pendlebury, S. R.; Grätzel, M.; Klug, D. R.; Durrant, J. R. *J. Am. Chem. Soc.* **2011**, *133*, 14868.

(27) Cummings, C. Y.; Marken, F.; Peter, L. M.; Tahir, A. A.; Wijayantha, K. G. U. *Chem. Commun.* **2012**, *48*, 2027.

(28) Surendranath, Y.; Kanan, M. W.; Nocera, D. G. *J. Am. Chem. Soc.* **2010**, *132*, 16501.

(29) Kanan, M. W.; Nocera, D. G. *Science* **2008**, *321*, 1072.

(30) Lutterman, D. A.; Surendranath, Y.; Nocera, D. G. *J. Am. Chem. Soc.* **2009**, *131*, 3838.

(31) Hong, Y.-R.; Liu, Z.; Al-Bukhari, S. F.; Lee, C. J.; Yung, D. L.; Chi, D.; Hor, T. S. *Chem. Commun.* **2011**, *47*, 10653.

(32) Pilli, S. K.; Deutsch, T. G.; Furtak, T. E.; Turner, J. A.; Brown, L. D.; Herring, A. M. *Phys. Chem. Chem. Phys.* **2012**, *14*, 7032.

(33) Abdi, F. F.; van de Krol, R. *J. Phys. Chem. C* **2012**, *116*, 9398.

(34) Zhong, D. K.; Choi, S.; Gamelin, D. R. *J. Am. Chem. Soc.* **2011**, *133*, 18370.

(35) Seabold, J. A.; Choi, K.-S. *Chem. Mater.* **2011**, *23*, 1105.

(36) Steinmiller, E. M. P.; Choi, K.-S. *Proc. Natl. Acad. Sci. U.S.A.* **2009**, *106*, 20633.

(37) Pijpers, J. J. H.; Winkler, M. T.; Surendranath, Y.; Buonassisi, T.; Nocera, D. G. *Proc. Natl. Acad. Sci. U.S.A.* **2011**, *108*, 10056.

(38) Barroso, M.; Mesa, C. A.; Pendlebury, S. R.; Cowan, A. J.; Hisatomi, T.; Sivula, K.; Grätzel, M.; Klug, D. R.; Durrant, J. R. *Proc. Natl. Acad. Sci. U.S.A.* **2012**, DOI: 10.1073/pnas.1118326109.

(39) Martinson, A. B. F.; DeVries, M. J.; Libera, J. A.; Christensen, S. T.; Hupp, J. T.; Pellin, M. J.; Elam, J. W. *J. Phys. Chem. C* **2011**, *115*, 4333.

(40) George, S. M. *Chem. Rev.* **2010**, *110*, 111.

(41) Klahr, B. M.; Martinson, A. B. F.; Hamann, T. W. *Langmuir* **2011**, *27*, 461.

(42) Klahr, B.; Giménez, S.; Fabregat-Santiago, F.; Bisquert, J.; Hamann, T. *Energy Environ. Sci.* **2012**, *5*, 7626.

(43) Klahr, B.; Gimenez, S.; Fabregat-Santiago, F.; Hamann, T.; Bisquert, J. *J. Am. Chem. Soc.* **2012**, *134*, 4294.

(44) McAlpin, J. G.; Surendranath, Y.; Dinca, M.; Stich, T. A.; Stoian, S. A.; Casey, W. H.; Nocera, D. G.; Britt, R. D. *J. Am. Chem. Soc.* **2010**, *132*, 6882.

(45) Symes, M. D.; Surendranath, Y.; Lutterman, D. A.; Nocera, D. G. *J. Am. Chem. Soc.* **2011**, *133*, 5174.

(46) Sanchez, H. L.; Steinfink, H.; White, H. S. *J. Solid State Chem.* **1982**, *41*, 90.

(47) Klahr, B. M.; Hamann, T. W. *Appl. Phys. Lett.* **2011**, *99*, 3.

(48) Bertoluzzi, L.; Bisquert, J. *J. Phys. Chem. Lett.* **2012**, *3*, 2517.

(49) Kanan, M. W.; Surendranath, Y.; Nocera, D. G. *Chem. Soc. Rev.* **2009**, *38*, 109.

(50) Pendlebury, S. R.; Cowan, A. J.; Barroso, M.; Sivula, K.; Ye, J.; Gratzel, M.; Klug, D. R.; Tang, J.; Durrant, J. R. *Energy Environ. Sci.* **2012**, *5*, 6304.

(51) Braun, A.; Sivula, K.; Bora, D. K.; Zhu, J.; Zhang, L.; Grätzel, M.; Guo, J.; Constable, E. C. *J. Phys. Chem. C* **2012**, *116*, 16870 DOI: 10.1021/jp304254k.

(52) Hellman, A.; Pala, R. G. S. *J. Phys. Chem. C* **2011**, *115*, 12901.

(53) Trainor, T. P.; Chaka, A. M.; Eng, P. J.; Newville, M.; Waychunas, G. A.; Catalano, J. G.; Brown, G. E., Jr. *Surf. Sci.* **2004**, *573*, 204.